JOURNAL OF MATERIALS SCIENCE 31 (1996) 6571–6576

Material flow under an indentor in indium phosphide

E. LE BOURHIS*, J. P. RIVIERE‡, A. ZOZIME‡
C.N.R.S., Laboratoire de Physique des Matériaux, 1, Place A. Briand, 92195 Meudon Cedex, France

Single crystals of indium phosphide, oriented in the ⟨0 0 1⟩ direction and at the temperature of 400 °C, have been deformed by a Vickers indentor. The generation and the development of the dislocations was deduced from the topographical observations of the deformed samples. The dislocation distribution under the indented surface was explained taking into account the dislocation interactions. Finally, both aspects have allowed a greater understanding of material flow under the indentor to be presented.

1. Introduction

In the field of semiconductor studies, the indentation test has been used to elucidate the inter-relationship between mechanical and electrical properties. This test has been applied to generate dislocations of known type in order to study their electrical activity [1–3] or to determine which type of dislocations, α or β, is the fastest [4]. Much work has been done to link the measured characteristics (hardness, rosette arm length) to the deformation temperature [5], the doping [6], surface type [7] and indentor orientation [8]. To understand the results, the stress field of the indentor was calculated by elastic [7] and elasto-plastic approaches [9]. This is tedious work because of the complexity and the high intensity of the stress field. The case of a {1 1 1} surface type of GaAs and CdTe deformed by a Vickers' indentor has been investigated in detail [7, 10]. The dislocation distribution at the surface and under the indentation was observed and it was shown how dislocations were generated and interacted in {1 1 1} planes. Roberts *et al.* [8, 11] investigated the case of a {0 0 1} face of GaAs deformed by a Knoop indentor by an approach similar to that given by Hirsch *et al.* [7]. The non-existence of rosette arms and the lower hardness when the indentor was parallel to a ⟨1 1 0⟩ direction was explained. We have investigated the case of a {0 0 1} surface of InP deformed by a Vickers' indentor, a particular behaviour has been observed and is discussed here.

2. Experimental procedure

2.1. Sample preparation

The two types of Czochalski grown single crystals of indium phosphide were ⟨0 0 1⟩ oriented. One of them was undoped ($n = 5 \times 10^{15}$ cm^{-3}), the other one was highly doped ($n = 5 \times 10^{18}$ cm^{-3}) with sulphur. The samples were mechanically–chemically polished with a 1% bromine–methanol solution.

The samples were deformed by a Vickers' indentor at 400 °C in an air atmosphere. Two orientations of the Vickers' indentor were used. In the 1 1 0 orientation of the indentor, they were parallel to ⟨1 1 0⟩ directions (see Fig. 1 below); in the 1 0 0 orientation of the indentor, the edges of the indentor were parallel to ⟨1 0 0⟩ directions (see Fig. 3 below). The approach speed of the indentor was 0.9 mm min^{-1}. The applied strength on the indentor was 1 N. The indentor was left 30 s on the sample before being raised.

2.2. Observation of the samples

The samples have been observed directly after deformation by optical microscopy (OM) and interferential optical microscopy (IOM) with a green light lamp ($\lambda = 0.54$ μm). They were also observed by scanning electron microscopy in the cathodoluminescence mode (CL) using a S20R detector. To investigate the dislocation distribution under the indented surface, the samples were chemically etched by a bromine–methanol solution. The etched depth was measured by optical microscopy, comparing the level of the stage of the microscope when focusing either on the etched zone or on the sample surface parts protected from the chemical etching.

The indented samples were also cleaved along the ⟨1 1 0⟩ direction to obtain cross-sectional views of the plastic zone.

3. Results

3.1. Topographical observation

3.1.1. 1 1 0 orientation of the indentor

The surface of the sample after deformation is shown in Fig. 1a. Cracks are observed, because InP samples

* *Present address*: Saint Gobain Recherche, 39, Quai Lucien Lefranc, BP 135F, 93303 Aubervillers Cedex, France.
‡ *Present address*: C.N.R.S., Laboratoire de Physique des Solides de Bellevue, 1, Place A. Briand, 92195 Meudon Cedex, France.

0022–2461

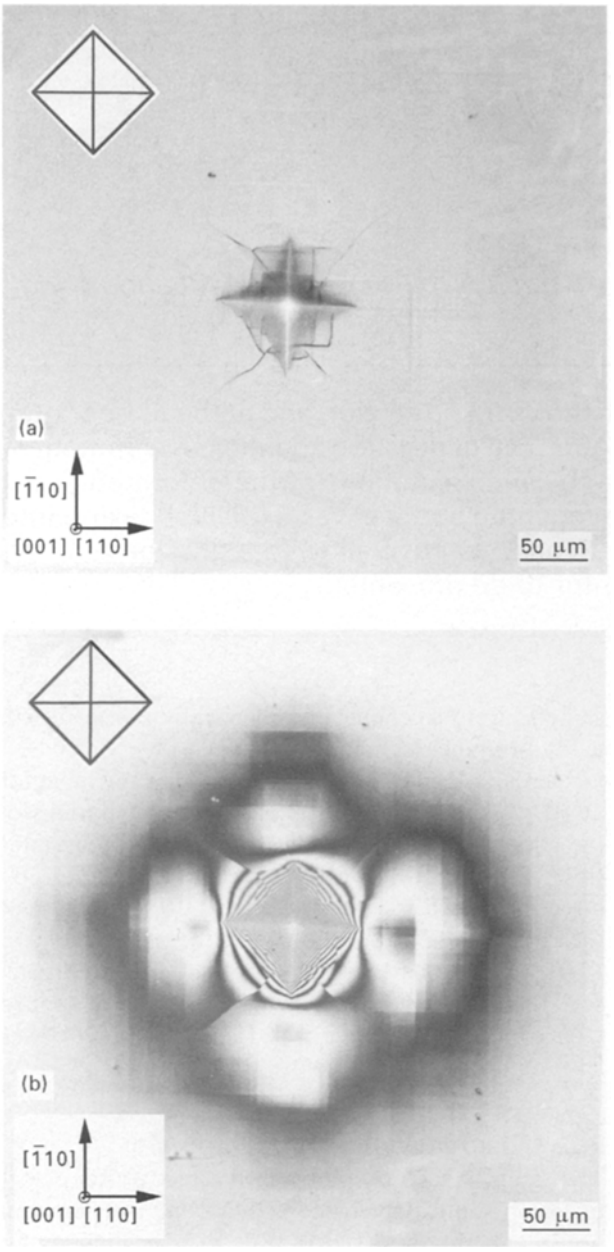

Figure 1 (a) Optical micrograph and (b) interferogram of the indented surface in undoped InP with a 1 1 0 orientation of the indentor. The indentor orientation is shown schematically on the left.

are still brittle at temperatures of 400 °C. It is not simple cleavage but is dislocation driven [12]. The samples are also plastically deformed: the indentor punches its shape and slip lines parallel to ⟨1 1 0⟩ directions are seen around the indentation. The ⟨1 1 0⟩ directions correspond to intersections of {1 1 1} slip planes with the (0 0 1) sample surface. To understand the way the indentor penetrates the sample, the form of the indentation is now described in detail.

At the beginning of the deformation, which corresponds to the deeper part of the indentation, the material is punched according to the shape of the indentor. The isolevel lines visualized by the interference lines on Fig. 1b are parallel to the indentor sides. At the end of the deformation, which corresponds to the higher part of the indentation, the material is pushed in a surface circumscribed to the section of the indentor. In fact, the isolevel lines progressively

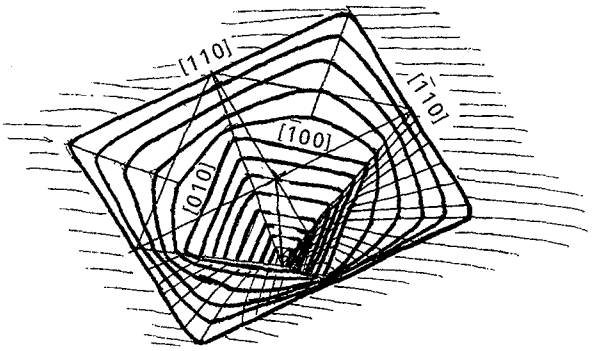

Figure 2 Indentation shape in the 1 1 0 orientation of the indentor deduced from Fig. 1b showing the two deformation regimes.

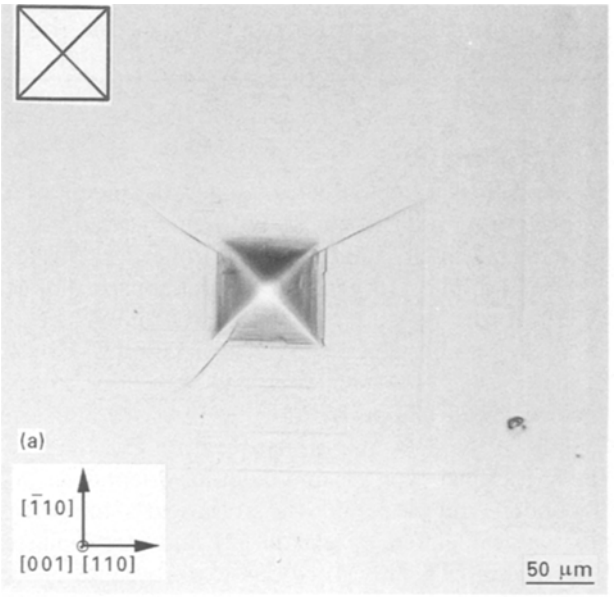

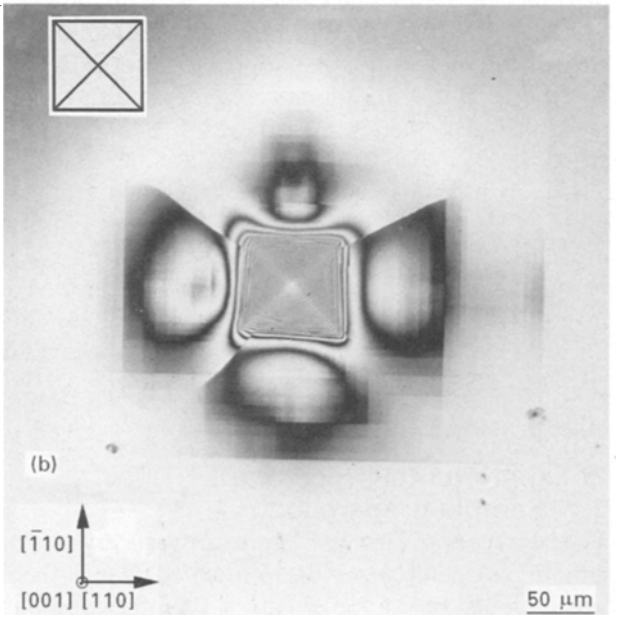

Figure 3 (a) Optical micrograph and (b) interferogram of the indented surface in undoped InP with a 1 0 0 orientation of the indentor. The indentor orientation is shown schematically on the left.

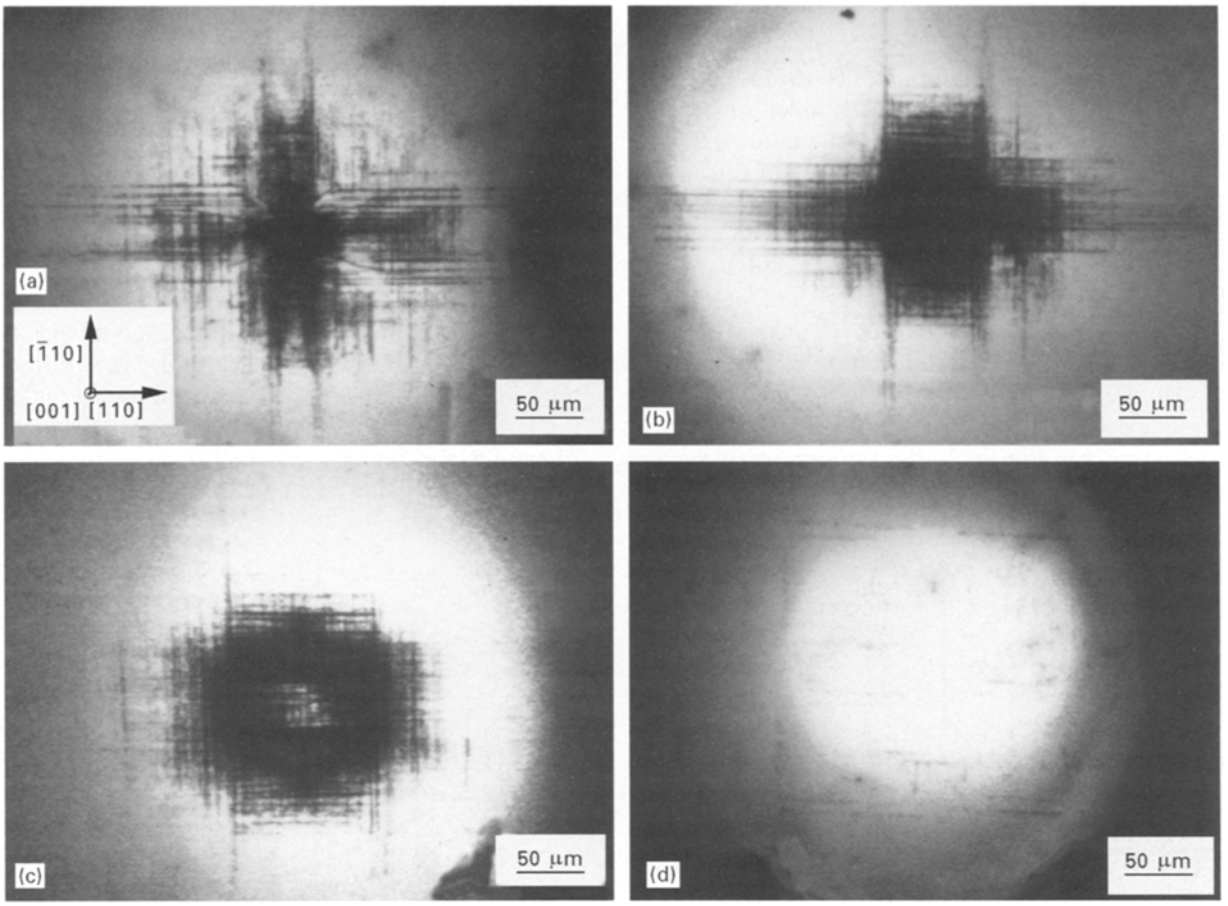

Figure 4 CL micrograph of the plastic zone obtained at different depths, p, under the indented surface in sulphur-doped InP with a 1 1 0 orientation of the indentor, (accelerating voltage 15 kV). p = (a) 0 μm, (b) 15 μm, (c) 30 μm, (d) 70 μm.

change from ⟨1 0 0⟩ directions parallel to the indentor sides, to ⟨1 1 0⟩ directions parallel to the slip lines already mentioned (Fig. 1a). In Fig. 2, the indentation shape is drawn and the two deformation regimes are clearly seen.

3.1.2. 1 0 0 orientation of the indentor

The deformed surface is shown in Fig. 3a and b. Cracks, and slip lines parallel to ⟨1 1 0⟩ directions are also visible. The isolevel lines keep parallel to ⟨1 1 0⟩ directions from the deeper part of the indentation to the external part.

3.2. Dislocation distribution

CL views of the plastic zone at increasing depths under the indented surface are shown in Fig. 4. Fig. 4a shows the dislocation distribution in a rosette at the surface of the sample. The rosette arms were still visible at a depth of 15 μm in Fig. 4b and progressively vanish at 30 and 70 μm. In fact, the plastic zone is composed of the rosette arms which correspond to material flow at the surface of the sample detailed elsewhere [13, 14], and a deeper zone which corresponds to material flow in the depth of the sample and is the object of this article. This region becomes larger when the depth is increased (see Fig. 4c and d). The CL contrast (the dislocation density) decreased when the depth was increased. In Fig. 4d the dislocations are much less visible; a square structure can be seen. In the deep plastic zone centre, the dislocation density decreased more rapidly than in its borders, as the dislocations are distributed in a roof structure (Fig. 5). Each of the roof sides is composed of several dislocation bands contained in {1 1 1} slip planes. The roof sides have a width of approximately 40 μm which is equivalent to the size of the indentation.

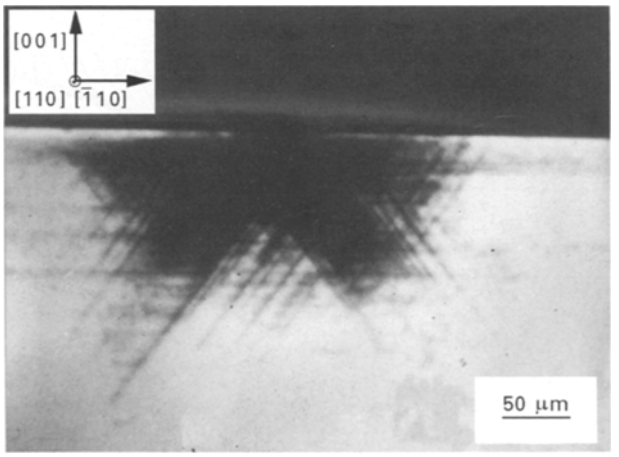

Figure 5 CL {1 1 0} plan view of the deep plastic zone in sulphur-doped InP.

4. Discussion

4.1. Dislocation generation

Two deformation regimes are occurring. The first regime is violent, during which the indentor punches its shape whatever the sample orientation may be. Such punching is shown schematically in Fig. 6. The planes pushed in the sample can be considered to be surrounded by hypothetical dislocation loops with vertical Burgers vectors $\boldsymbol{b} = a[00\bar{1}]$ and with line direction parallel to the sides of the indentor. Note that we did not observe these hypothetical dislocations but they will help in understanding the material flow. In the 1 1 0 orientation of the indentor the dislocation lines are parallel to $\langle 100 \rangle$ directions as shown schematically in Fig. 7a. In the 1 0 0 orientation of the indentor they are parallel to $\langle 110 \rangle$ directions (see Fig. 7b). These hypothetical dislocations with large Burgers vectors gliding in planes of narrow interplanar spacing are very unstable and split into two dislocations with Burgers vector $a/2\langle 101 \rangle$ inclined to the surface and slipping in two $\{111\}$ different planes as shown in Fig. 7a and b. The dissociation reaction can be written $a[00\bar{1}] = a/2[0\bar{1}\bar{1}] + a/2[01\bar{1}]$. The sharing line is along the $\langle 110 \rangle$ direction common with the two $\{111\}$ slip planes of the dislocations. In the 1 1 0 orientation of the indentor, the dissociation lines are inclined to the surface (Fig. 7a), whereas in the 1 0 0 orientation of the indentor they are parallel to the surface (Fig. 7b). After dissociation, the dislocations may slip under the indentor on converging or diverging slip planes (see Fig. 8). Their slip planes are

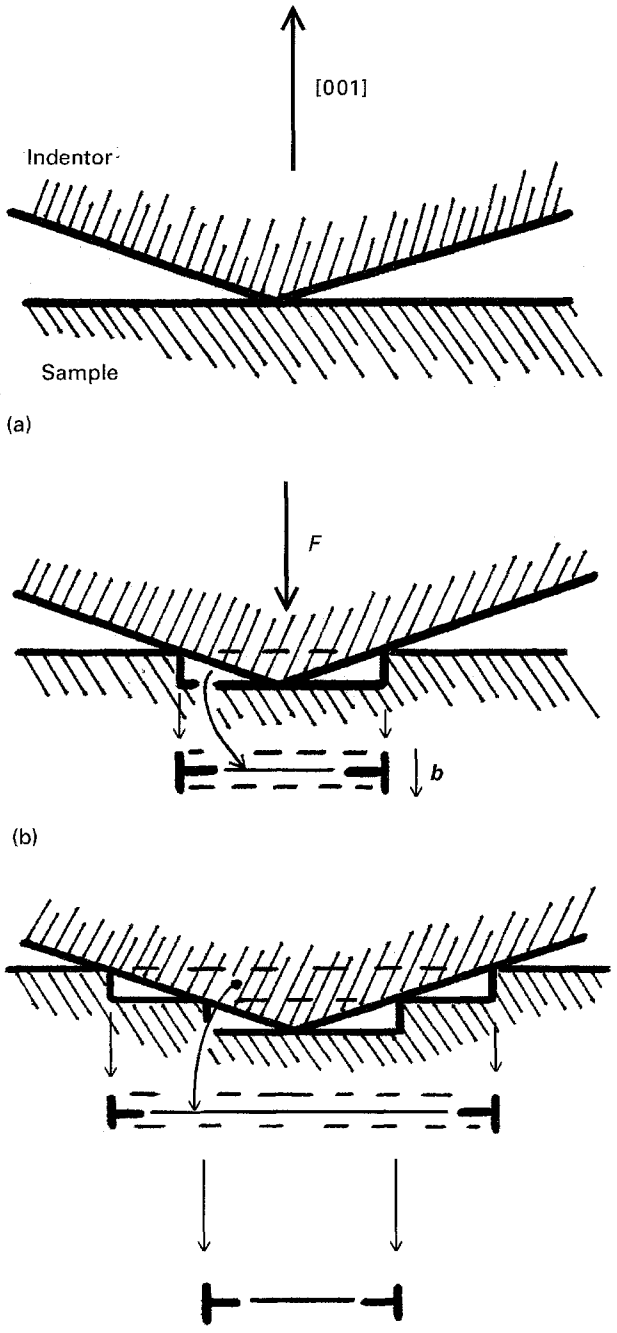

Figure 6 General punching mechanism by the generation of dislocation loops with a vertical Burgers vector.

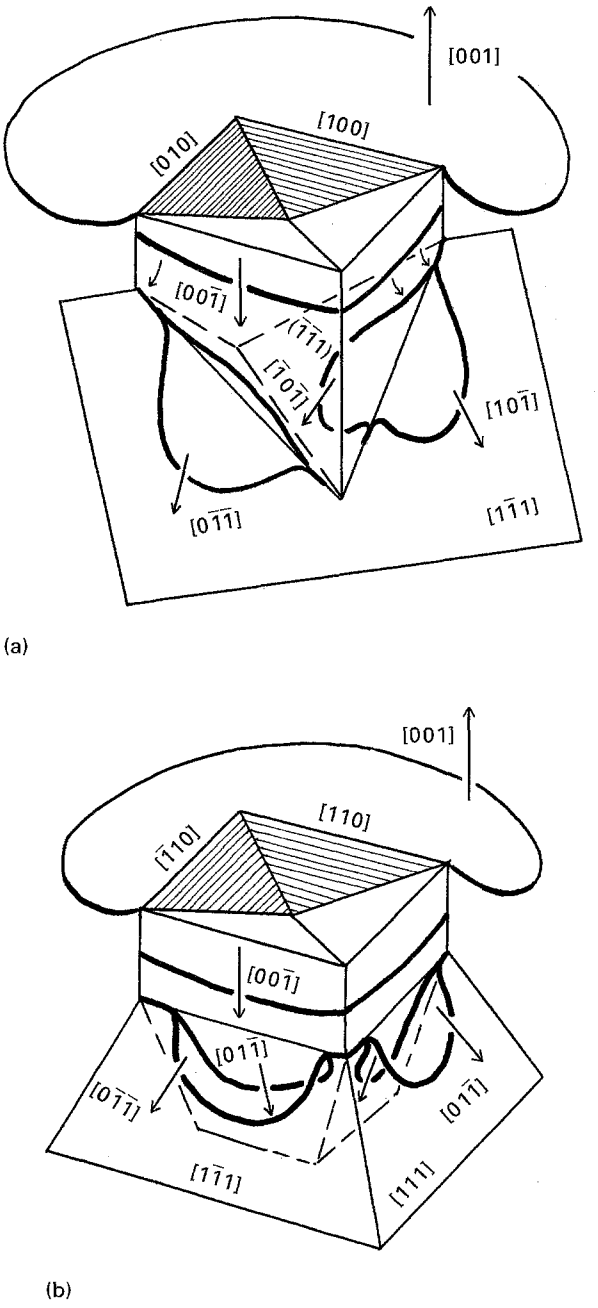

Figure 7 Generation and decomposition of dislocation loops with a Burgers vector $\boldsymbol{b} = a[00\bar{1}]$ at the beginning of the deformation (first deformation regime). (a) 1 1 0 orientation of the indentor, (b) 1 0 0 orientation of the indentor.

called, respectively, internal planes and external planes.

At the end of the deformation (second deformation regime) dislocations of Burgers vectors $\boldsymbol{b} = a/2\langle 1\,1\,0\rangle$ inclined to the surface are directly generated at the immersion of the indentor. In the 1 1 0 orientation of the indentor, they are generated at the edges of the indentor (point A in Fig. 9a). In the 1 0 0 orientation of the indentor, they are generated along the sides of the indentor (Fig. 9b). These dislocations slip on external $\{1\,1\,1\}$ slip planes which generate more deformation. The material is then pushed in a surface bordered by $\langle 1\,1\,0\rangle$ directions that correspond to the intersection of the external $\{1\,1\,1\}$ slip planes and the $\{0\,0\,1\}$ surface plane. In the 1 1 0 orientation of the indentor, the two regimes can be distinguished (see Fig. 1b) because, during the first regime, the sides of the indentor are along $\langle 1\,0\,0\rangle$ directions (compare Figs. 7a and 9a). In the case of the 1 0 0 orientation of the indentor, the two regimes are activated along a same line $\langle 1\,1\,0\rangle$ (see Fig. 3b and compare Figs. 7b and 9b) and cannot be distinguished.

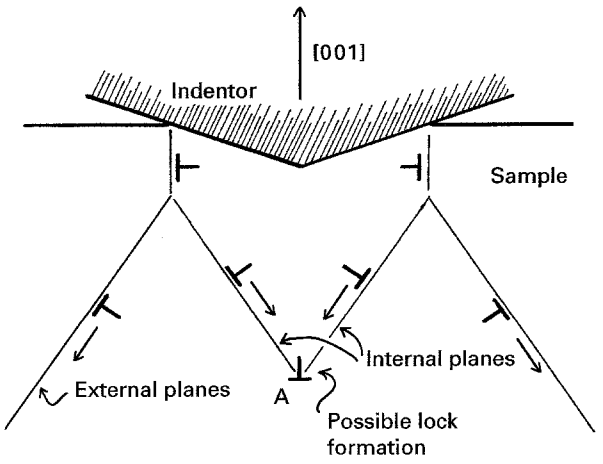

Figure 8 Configuration of the internal and external $\{1\,1\,1\}$ slip planes. Possible lock formation at A.

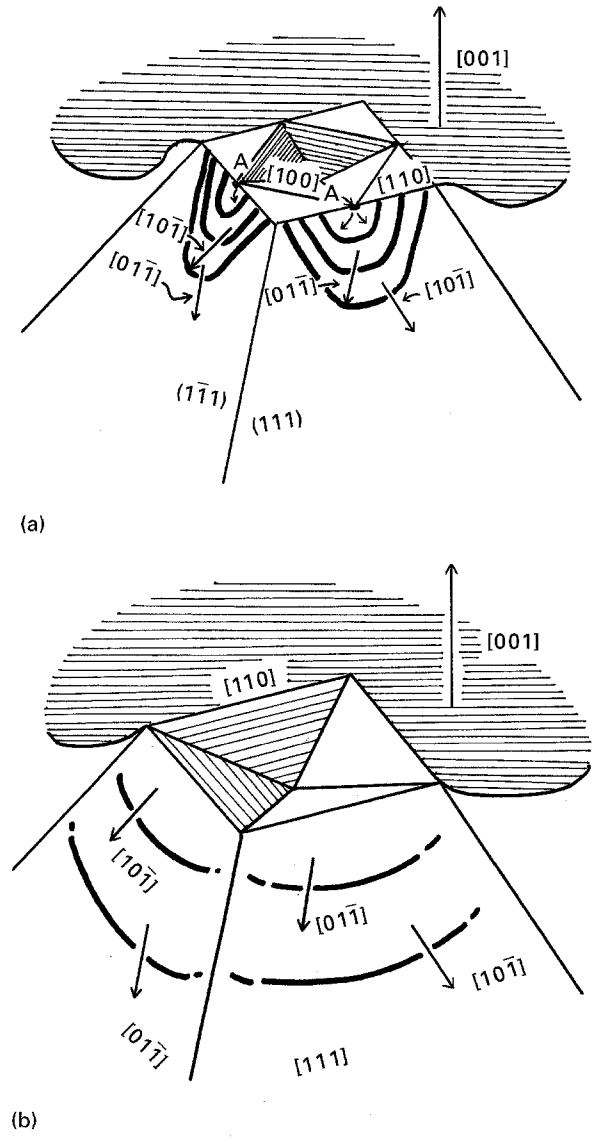

Figure 9 Generation of dislocation loops with Burgers vector $\boldsymbol{b} = a/2\langle 1\,1\,0\rangle$ inclined to the surface of the sample (second deformation regime). (a) 1 1 0 orientation of the indentor, (b) 1 0 0 orientation of the indentor.

4.2. Deep plastic zone structure

In the former paragraph, two dislocation generation regimes were distinguished. During the first regime, both internal and external $\{1\,1\,1\}$ slip planes are activated, whereas only external $\{1\,1\,1\}$ slip planes are activated during the second regime. Interaction between internal planes may lead to work-hardening by forming Lomer Cottrell locks at point A in Fig. 8, as mentioned elsewhere [8]. Consequently, dislocations gliding on $\{1\,1\,1\}$ internal planes cannot penetrate in the sample very much and the dislocations that penetrate deeper in the material are those gliding on external $\{1\,1\,1\}$ slip planes.

In Fig. 10, two dislocation loops, AB and CD, with the same Burgers vector inclined to the sample surface, are represented in step I. They are gliding in two

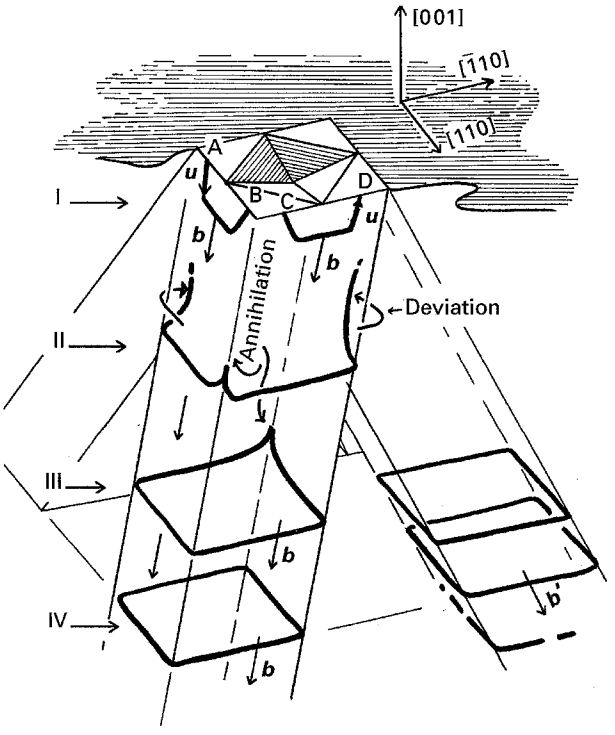

Figure 10 Propagation of dislocation loops along the four $\langle 1\,1\,0\rangle$ inclined directions to the sample surface.

{1 1 1} external slip planes. In step II, the annihilation of dislocation segments at the intersection of their glide planes is quite likely to reduce their elastic energy. The cross-slip of the screw segments and the last annihilation in step III finally lead to dislocation loops gliding along the direction parallel to the Burgers vector (step IV).

4.3. Plastic zone extension

The dislocation loops gliding along each of the four ⟨1 1 0⟩ directions penetrate in the material, owing to their mutual repulsion. The effect of the stress field of the indentor on the dislocation equilibrium was neglected, because it is mainly a compressive radial stress field and does not act on dislocations of quasi radial Burgers vectors [13]. During the second deformation regime, dislocations are only generated in close external {1 1 1} slip planes where dislocations are not yet numerous. On the other hand, the tangled dislocations under the indentor prevent the main part of the dislocation from returning to the surface when the indentor is raised up. A simple estimation of the dislocation loop number, n, generated during the second deformation regime is possible knowing the pushed depth, h, corresponding to this regime (Fig. 1b). Because there are four gliding directions, the dislocation loop number, n, is given by

$$n = \frac{h}{4\boldsymbol{b}_{[0\,0\,1]}} \quad (1)$$

where $\boldsymbol{b}$ is the Burgers vector of the dislocations and $\boldsymbol{b}_{[0\,0\,1]}$ its vertical component. The total length, L, of the n dislocation loop distribution was calculated with a model similar to that described in the literature for the equilibrium of linear arrays of dislocations [15, 16]. We assumed that at equilibrium the mutual repulsion stress field between dislocations is balanced by the critical stress necessary to move a dislocation [13, 17]. We took, for the critical stress, the critical resolved shear stress (CRSS) determined by compression tests [18, 19]. The results given in Table I show that there is good agreement between the calculated length and the plastic zone extension.

5. Conclusion

Dislocations are generated at the immersion of the indentor because of the high shear stress at this singular point. Two deformation regimes were distinguished. At the beginning of the deformation (first deformation regime) when the material is punched, the generated dislocations with Burgers vector inclined to the surface sample are gliding on external and internal {1 1 1} slip planes, whereas at the end of the deformation (second deformation regime) they are gliding only on external planes. Internal gliding leads to work-hardening so that the dislocations gliding on external {1 1 1} slip planes penetrate deeper into the sample.

TABLE I Results of the calculation of the number, n, of dislocation loops generated during the second deformation regime and the length, L, of a distribution of 400 dislocation loops 40 μm large, in undoped and sulphur-doped InP

	h (μm)	n Equation 1	CRSS at 400 °C (MPa)	L (μm)
Undoped InP	0.81	690	11 [18]	100
S-doped InP	0.40	350	22 [19]	85

The deep plastic zone structure is explained by the interaction between the generated dislocations which lead to four dislocation loop "pile ups" parallel to ⟨1 1 0⟩ directions inclined to the surface. A good estimation of the plastic zone extension can be made by taking into account the CRSS and the elastic forces between the dislocation loops generated during the second deformation regime.

References

1. A. ZOZIME, I. HANKE and W. SCHRÖTER, *Phys. Status Solidi* **138a** (1993) 445.
2. T. WOSINSKI, A. ZOZIME, A. RIVIÈRE and C. VERMELIN, *ibid.* **142a** (1994) 347.
3. B. SIEBER, J. L. FARVACQUE and A. MIRI, *ibid.* **138a** (1993) 673.
4. P. D. WARREN, P. PIROUZ and S. G. ROBERTS, *Phil. Mag.* **50A** (1984) L23.
5. A. FISSEL and M. SCHENK, *J. Mater. Sci. Mater. Elec.* **3** (1992) 147.
6. D. ARIVUOLI, R. FORNARI and J. KUMAR, *J. Mater. Sci. Lett.* **10** (1991) 559.
7. P. B. HIRSCH, P. PIROUZ, S. G. ROBERTS and P. D. WARREN, *Phil. Mag.* **52B** (1985) 759.
8. S. G. ROBERTS, P. D. WARREN and P. B. HIRSCH, *J. Mater. Res.* **1** (1986) 162.
9. K. L. JOHNSON, *J. Mech. Phys. Solids* **18** (1970) 115.
10. A. RIVIÈRE, B. SIEBER and J. P. RIVIÈRE, *Micros. Microanal. Microstruct.* **2** (1991) 503.
11. S. G. ROBERTS, P. D. WARREN and P. B. HIRSCH, *Mater. Sci. Eng.* **A105/106** (1988) 19.
12. M. M. CHAUDHRI, *Phil. Mag. Lett.* **53** (1986) L55.
13. E. LE BOURHIS, Thesis, Paris VII (1994).
14. E. LE BOURHIS, A. RIVIÈRE, J. P. RIVIÈRE and A. ZOZIME, to be published.
15. J. D. ESHELBY, F. C. FRANK and F. R. N. NABARRO, *Phil. Mag.* **42** (1951) 351.
16. S. G. ROBERTS, P. PIROUZ and P. B. HIRSCH, *J. Phys. C4* **44** (1991) 75
17. A. ZOZIME, E. LE BOURHIS, H. HEDEMANN, C. VERMEULIN and J. P. RIVIÈRE, to be published.
18. E. LE BOURHIS, A. ZOZIME, A. RIVIÈRE and C. VERMEULIN, *J. Phys. III* **5** (1995) 1795.
19. P. GALL, Thesis, Institut national des sciences appliquées de Toulouse (1985).

Received 25 May 1995
and accepted 2 July 1996